Journal of Controlled Release 163 (2012) 75–81

Contents lists available at SciVerse ScienceDirect

Journal of Controlled Release

journal homepage: www.elsevier.com/locate/jconrel

Image-guided, targeted and triggered drug delivery to tumors using polymer-based microbubbles

Stanley Fokong [a], Benjamin Theek [a], Zhuojun Wu [a,b], Patrick Koczera [a], Lia Appold [a], Samuel Jorge [a], Ute Resch-Genger [c], Marc van Zandvoort [b,d], Gert Storm [e,f], Fabian Kiessling [a,*], Twan Lammers [a,e,f,*]

[a] Department of Experimental Molecular Imaging, University Clinic and Helmholtz Center for Biomedical Engineering, RWTH — Aachen University, Aachen, Germany
[b] Institute of Molecular Cardiology, University Clinic, RWTH — Aachen University, Aachen, Germany
[c] Federal Institute for Materials Research and Testing (BAM), Division Biophotonics, Berlin, Germany
[d] Department of Biomedical Engineering, Maastricht University Medical Centre, Maastricht, The Netherlands
[e] Department of Pharmaceutics, Utrecht University, Utrecht, The Netherlands
[f] Department of Targeted Therapeutics, MIRA Institute for Biomedical Technology & Technical Medicine, University of Twente, Enschede, The Netherlands

ARTICLE INFO

Article history:
Received 27 February 2012
Accepted 2 May 2012
Available online 9 May 2012

Keywords:
Ultrasound
Microbubbles
Fluorescent reporter
Drug delivery
Tumor targeting
Theranostics

ABSTRACT

Microbubbles (MB) are routinely used contrast agents for functional and molecular ultrasound (US) imaging. In addition, they have been attracting more and more attention for drug delivery purposes, enabling e.g. US-mediated drug delivery across biological barriers and US-induced triggered drug release from the MB shell. The vast majority of efforts in this regard have thus far focused on phospholipid-based soft-shell MB, which are suboptimal for stably incorporating large amounts of drug molecules because of their relatively thin shell. Using poly(butyl cyanoacrylate) (PBCA)-based hard-shell MB, we show here that both hydrophilic (Rhodamine-B) and hydrophobic (Coumarin-6) model drugs can be efficiently and stably entrapped within the ~50 nm shell of PBCA MB. In addition, we demonstrate that model drug loading does not negatively affect the acoustic properties of the MB, and that functionalizing the surface of fluorophore-loaded MB with anti-VEGFR2 antibodies enables image-guided and targeted model drug delivery to tumor blood vessels. Finally, we show both in vitro and in vivo that disintegrating VEGFR2-targeted MB with high-mechanical index US pulses leads to high levels of model drug release. Consequently, these findings indicate that polymer-based MB are highly suitable systems for image-guided, targeted and triggered drug delivery to tumors and tumor blood vessels.

1. Introduction

The majority of routinely used chemotherapeutic agents suffer from poor pharmacokinetics and from an inappropriate biodistribution. Because of their low molecular weight, their high hydrophobicity and/or their instability, the tumor localization of i.v. administered chemotherapeutic agents tends to be low, while significant amounts accumulate in potentially endangered healthy tissues. To increase the tumor accumulation of i.v. administered chemotherapeutic drugs, to decrease their localization in healthy organs and tissues, and to thereby improve the balance between their efficacy and their toxicity, a large number of drug delivery systems have been designed and evaluated over the years. These formulations e.g. include liposomes, polymers, micelles and nanoparticles, which via the Enhanced Permeability and Retention (EPR) effect [1], enable a relatively selective delivery of chemotherapeutic drugs to tumors [2–7].

Besides such long-circulating 3–200 nanometer-sized carrier materials, also micro- and millimeter-sized drug delivery systems can be used to improve the efficacy of anticancer therapy. Regarding the latter, for instance, polyanhydride-based polymeric wafers containing carmustine are routinely implanted intra- or peri-tumorally for the post-surgical treatment of partially resectable brain tumors [8,9]. Regarding the former, several different 10–1000 μm-sized microspheres and drug-eluting beads have been designed and evaluated over the years, which upon subcutaneous, intratumoral and/or trans-arterial administration aim to assure sustained drug release and high drug levels in blood and/or in tumors [10,11].

In addition to this, also 1–5 μm-sized gas-filled microbubbles (MB), which are routinely used for functional and molecular ultrasound (US) imaging [12–14], can be employed to enhance drug delivery to tumors. This is because local US-induced MB oscillation (stable cavitation) or destruction (inertial cavitation), leads to a temporal permeabilization of blood vessels and/or cell membranes [15–23]. To exploit this potential of MB for facilitating drug delivery across

* Correspondence to: F. Kiessling and T. Lammers: Department of Experimental Molecular Imaging, RWTH — Aachen University, Aachen, Germany.
E-mail addresses: fkiessling@ukaachen.de (F. Kiessling), tlammers@ukaachen.de (T. Lammers).

0168-3659/$ – see front matter © 2012 Elsevier B.V. All rights reserved.
doi:10.1016/j.jconrel.2012.05.007

biological barriers, therapeutic agents can either be co-administered with MB [24,25], or loaded into the shell of MB [13,26,27]. In addition to enhancing drug targeting to tumors, combining MB with US has also been extensively used for thrombolysis and for enabling drug delivery across the blood–brain-barrier [28–31].

Thus far, the vast majority of studies in which MB have been used to enable or to enhance drug delivery across biological barriers have focused on phospholipid-based soft-shell MB [15–23,26,28]. These MB, however, suffer from several important shortcomings, including e.g. their relatively low stability, their inability to encapsulate high amounts of drug within their thin shell (~3 nm), the fact that drug loading tends to be unstable, and the notion that only highly hydrophobic drugs can be incorporated efficiently [15–23]. Pioneering efforts to use polymer-based hard-shell MB for drug delivery purposes have recently been reported by Wheatley and colleagues, who incorporated doxorubicin and paclitaxel into poly(lactic acid) (PLA) -based MB, and showed that these formulations can be used to stably encapsulate relatively high amounts of these two chemotherapeutic drugs within their 100–150 nm-thick polymeric shell [32–34]. Furthermore, they demonstrated that hydrophobic drugs are entrapped more efficiently than hydrophilic drugs, that drug incorporation does not negatively affect the acoustic properties of the MB, and that upon exposure to destructive US pulses, the MB efficiently release the encapsulated agents, thereby killing cancer cells in vitro [34].

We here extend these efforts to the in vivo situation, using antibody-targeted and model drug-loaded poly(butyl cyanoacrylate) (PBCA) MB. PBCA MB are known to be highly suitable for molecular imaging purposes [14,35–37]. They have a shell-thickness of ~50 nm [38], and they therefore likely possess a much higher drug-loading capacity than do phospholipid-based soft-shell MB. Two different fluorescent model drugs were used for this purpose, i.e. Rhodamine-B, which is relatively hydrophilic (logP = 1.95), and Coumarin-6, which is relatively hydrophobic (logP = 5.43). As exemplified by Fig. 1, these two model drugs were incorporated into the shell of PBCA MB using two different procedures, i.e. either by already introducing them during MB synthesis (1-step loading), or by incubating them with preformed MB (i.e. 2-step loading).

Following model drug encapsulation, the MB were surface-modified with antibodies against the vascular endothelial growth factor receptor 2 (VEGFR2; which is highly overexpressed on angiogenic endothelium), in order to specifically target them to tumor blood vessels. The payload of both model drugs in the MB shell before and after surface-modification was evaluated, as was their release upon exposure to destructive US pulses. Furthermore, the effect of model drug loading on the acoustic properties of the MB was investigated. Finally, as exemplified by Fig. 2, fluorophore-loaded and VEGFR2-antibody-containing MB were injected i.v., and were used to selectively bind to and release model drugs in tumor blood vessels, to thereby enable image-guided, targeted and triggered drug delivery.

2. Materials and methods

2.1. Materials

n-Butylcyanoacrylate (BCA) was purchased from Special Polymer Ltd (Bulgaria). Triton X-100, Dimethylformamide (DMF), Rhodamine-B, Coumarin-6 and 1-ethyl-3-(3-dimethylaminopropyl)carbodiimide (EDC) were obtained from Sigma-Aldrich (Germany). Streptavidin was purchased from Calbiochem (Germany). Deionized water was used for all experiments and all reagents were of appropriate analytical grade.

2.2. Microbubble synthesis

Fluorophore-loaded poly(n-butyl cyanoacrylate) (PBCA) microbubbles (MB) were prepared by slightly modifying the established emulsion polymerization technique used for synthesizing PBCA MB [38,39]. Two fluorescent dyes (i.e. Rhodamine-B and Coumarin-6) were used as hydrophilic and hydrophobic model drugs, respectively, and were incorporated into the shell of the MB. As exemplified by Fig. 1, this was done both, via a 1-step and via a 2-step (post-loading) procedure.

In the 1-step procedure, the model drugs (dissolved in 300 μL of water (Rhodamine-B) or DMF (Coumarin-6)) were introduced during the polymerization process, in which 3 mL of monomeric n-butyl cyanoacrylate (BCA) were added drop-wise to 300 mL of an aqueous solution containing 1% Triton X-100 at pH 2.5. Using an Ultra-Turrax T 50 basic (IKA-Werke, Germany), the mixture was then stirred for 60 min at 10,000 rpm, during which the MB formed and the model drugs were incorporated into the polymeric MB shell. The resulting MB suspension was washed 3–5 times by flotation, to remove non-entrapped/excess fluorophores and non-MB-associated polymer.

In the 2-step procedure, 300 μL of Rhodamine-B-containing water or Coumarin-6-containing DMF (at equivalent concentrations as used in the 1-step procedure) were added to 20 mL of preformed MB. This mixture was then stirred for 10 min using a magnetic stirrer, and purified by 3–5 flotation steps. To determine the most efficient way of drug loading, 4 different dye concentrations (0.2, 0.5, 1.5, and 5 mg) were used for both fluorophores. The resulting formulations were compared with regard to MB formation, encapsulation efficiency and drug release efficiency.

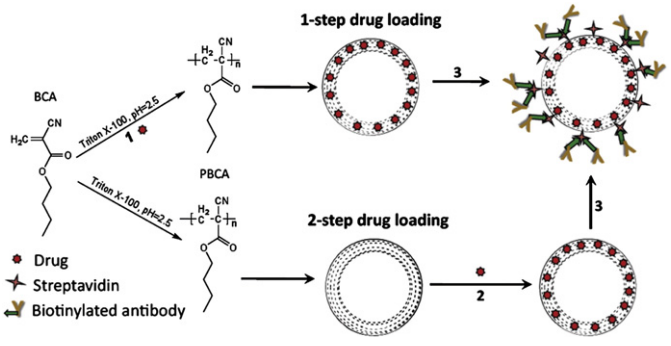

Fig. 1. Schematic representation of the preparation of model drug-loaded and VEGFR2-antibody-targeted PBCA MB. Rhodamine-B and Coumarin-6 were used as fluorescent model drugs, and they were loaded into MB either via a 1-step, or via a 2-step procedure. In the 1-step procedure, the fluorophores were introduced during MB synthesis (1). In the 2-step-procedure, the fluorophores were loaded into preformed MB (2). In both cases, fluorophore-loaded MB were finally hydrolyzed, surface-modified with streptavidin, and functionalized with biotinylated anti-VEGFR2-antibodies (3).

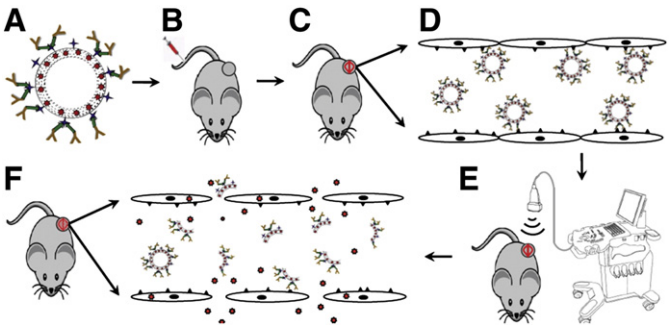

Fig. 2. Schematic setup for image-guided, targeted and triggered drug delivery to tumors using polymer-based MB. Fluorophore-loaded and VEGFR2-antibody-targeted MB (A) are injected i.v. (B), and upon binding to tumor blood vessels (C–D), high-mechanical index destructive US pulses are applied (E), to induced MB destruction and hence model drug release and extravasation into the tumor interstitium (F).

2.3. Synthesis of VEGFR2-targeted MB

To enable site-specific drug delivery to tumors, MB were surface-decorated with antibodies that recognize receptor structures over-expressed by angiogenic endothelium. This was done by exploiting the highly effective and highly selective interaction between streptavidin and biotin. To this end, fluorophore-loaded MB were initially surface-functionalized by treatment with 0.1 N NaOH, to introduce carboxyl groups. Subsequently, 5×10^8 surface-functionalized MB were incubated with 7.5 mg of EDC and 300 μg of streptavidin (in 10 mM sodium acetate buffer, pH 4.5) for 16 h at 4 °C. The streptavidin-coated MB were then purified by flotation, and their size distribution and concentration were determined using a Multisizer 3 (Beckmann Coulter). Finally, prior to injection, 50 μL of a solution containing 1×10^7 streptavidin-modified MB were incubated with 1.5 μL of 0.5 mg/mL solution of biotinylated anti-mouse VEGFR2 antibodies (Abcam, Germany) at room temperature for 5 min.

2.4. Two-photon laser scanning microscopy

The encapsulation of the two model drugs into the shell of the targeted MB was visually confirmed by two-photon laser scanning microscopy (TPLSM). To this end, 1×10^9 MB in 50 μL were immobilized on a coverslip using 50 μL Vectashield mounting media (Vector Labs, Germany). The MB were then visualized and analyzed using an Olympus FV1000MPE Multiphoton Microscopy System, equipped with a Mai TaiDeepSee pulsed Ti:Sapphire laser, at an excitation wavelength of 800 nm, using a 60× water dipping objective. One photo-multiplier tube was used to detect the fluorescence signals, and filters were adjusted to the corresponding emission spectra, i.e. 490–560 nm for Coumarin-6, and 560–600 nm for Rhodamine-B. Image processing and analysis were performed using the Image-Pro 3D analyzer 7.0 software (Media Cybernetics, Inc).

2.5. Quantification of model drug loading and encapsulation efficiency

Fluorescence spectroscopy was used to determine the amount of fluorophore encapsulated into the MB. First, using 10 different concentrations, standard curves were prepared for Rhodamine-B and Coumarin-6 (both in ethanol). Then, 1×10^9 MB were dissolved in 1 mL of ethanol (which dissolves the polymers, destroys the MB, and releases the total payload of encapsulated fluorophore). Using excitation and emission wavelengths of 540 and 580 for Rhodamine-B, and of 490 and 525 nm for Coumarin-6, the amounts of model drug incorporated were subsequently quantified using an Infinite 200 Pro plate reader (Tecan Group Ltd, Germany). Based on the analyses, the encapsulation efficiency (EE; defined as (the total amount of model drug incorporated/the total amount of model drug added)×100%) was determined for both dyes, all four model drug concentrations and both synthetic procedures.

2.6. Effect of antibody-functionalization on model drug encapsulation

The preparation of target-specific MB entails an initial hydrolysis of the fluorophore-loaded MB with 0.1 N NaOH, in order to introduce carboxyl groups on their surface. As this might lead to a loss of encapsulated model drugs, we investigated the impact of hydrolysis on the payload of the two fluorophores. To this end, the amounts of encapsulated model drugs in hydrolyzed MB were determined (using the fluorescence spectroscopy-based method described above), and were compared to those obtained for non-hydrolyzed MB.

2.7. Effect of model drug encapsulation on the acoustic properties of the MB

To analyze the effect of fluorophore encapsulation on the US contrast-enhancement characteristics of the MB, the acoustic properties of regular MB (without model drugs), 1- and 2-step fluorophore-loaded MB and hydrolyzed fluorophore-loaded MB were analyzed. This was done by suspending 1×10^8 MB of each formulation in a glass beaker containing 200 mL of water, and by imaging in non-linear contrast mode at a frequency of 18 MHz with a mechanical index (MI) of 0.2 (corresponding to 4% power), using a preclinical US device (Vevo 2100, VisualSonics, Canada). A region-of-interest (ROI) of ~500 mm^2 was then placed in the middle of the image, from which the contrast intensity of the different MB formulations was analyzed and their acoustic properties were compared.

2.8. Quantification of US-induced model drug release

MB exposure to high-mechanical-index US pulses leads to MB destruction and thereby likely also to significant model drug release. The percentages of encapsulated fluorophores released upon US-induced MB destruction were determined by means of the fluorescence spectroscopy-based method mentioned above. To induce model drug release, 1×10^9 of hydrolyzed MB were dispersed in 1 mL of water, and exposed to US for 10 min, to destroy all MB. The solution was subsequently centrifuged (Heraeus Fresco 21, ThermoScientific, Germany) at 2000 rpm for 5 min, after which the supernatant (containing released fluorophores) was separated from the polymer fragments at the bottom and analyzed spectrofluorometrically. Analogous to drug encapsulation, drug release was quantified using a standard curve, and it was expressed as percentage of the total amount of drug incorporated.

2.9. In vivo US imaging and triggered drug release

All animal experiments were approved by local and national authorities for animal care. After inoculating 1×10^6 CT26 mouse colon carcinoma cells subcutaneously into the flanks of six 8–10 week old mice, tumors were allowed to grow for 10 days, until they reached a size of ~6×6 mm. Animals were then anesthetized using isofluorane and US imaging and triggered drug delivery were performed using the Vevo 2100 imaging system with a MS250 transducer (VisualSonics, Canada), at a frequency of 18 MHz. The ultrasound pulse was transmitted with 6 cycles, with a peak negative pressure of approximately 600 kPa and a pulse repetition frequency (PRF) of 10 kHz. At 4% power, as was used for imaging, the mechanical index (MI) was 0.2. After focusing on the tumor in B-mode US imaging, 1×10^7 VEGFR2-targeted fluorophore-containing MB were injected i.v. via the tail vein. A total of three animals were used per MB formulation, and of these, one tumor-bearing mouse was used per experimental US condition (i.e. n = 1 for no US, n = 1 for continuous destruction (MI = 1.0) US, and n = 1 for 3 destructive pulses 7 min after i.v. injection; see below). The MB injection curve was recorded for 30 s in non-linear contrast mode (MI = 0.2), to validate efficient tumor perfusion and MB administration. Seven minutes after administration, the specific binding of the VEGFR2-targeted MB to tumor blood vessels was visualized (NB: the half-life time of MB is ~1 min), and MB were destroyed (MI = 1.0), to enable imaging and triggered drug release. The imaging sequence used was based on the analysis of several 2D frames before and after destructive pulses, and was followed by 3D destruction sequences over the entire tumor. Negative control mice did not receive any US. Positive control mice received US continuously for 7 min.

2.10. Fluorescence microscopy

Immediately after US imaging and MB destruction, animals were i.v. injected with 75 μL of FITC-labeled lectin (for mice treated with Rhodamine-loaded MB) or Rhodamine-lectin (for mice treated with Coumarin-loaded MB). Lectin (Ricinus Communis Agglutinin I, Vector Labs, Germany) was administered at a dose of 5 mg/kg, and was used to stain perfused blood vessels in vivo, thereby enabling fluorescence microscopy-based analyses of MB localization and model drug release

in blood vessels without the need for ex vivo antibody-based staining protocols (which might lead to the wash-out of the fluorophores released from MB). Fifteen minutes after lectin injection, the animals were sacrificed under deep anesthesia, and the tumors harvested and frozen in Tissue-Tek at −80 °C. Using a CM3050S Cryostat (Leica Microsystems GmbH, Germany), 7 μm thick sections were made, and without any further fixation or staining steps, they were analyzed using an Axio Imager M2 fluorescence microscope (Carl Zeiss AG, Germany) at a magnification of 200×. Image processing and analysis was performed using the ImageJ software (National Institute of Health, USA).

2.11. Statistical analysis

All results are presented as average ± standard deviation. Statistical significance was evaluated using the standard two-tailed student's *t* test. $p<0.05$ was considered to indicate significant differences.

3. Results and discussion

3.1. MB synthesis

The synthesis of model drug-containing PBCA MB was successful for Rhodamine-B and Coumarin-6, using both the 1-step and 2-step procedure. At a concentration of 15 mg, however, 1-step drug loading interfered with MB formation (data not shown). Coulter counter-based particle size analyses showed no substantial differences in size distribution between fluorophore-loaded and non-loaded MB, with average sizes always around 1.5 μm with relatively low polydispersity. This indicates that at amounts of up to 5 mg, both model drugs did not interfere with MB formation, irrespective of whether they are hydrophilic or hydrophobic, and irrespective of whether they were added during MB synthesis (1-step) or afterwards (2-step). This is in line with the results obtained for doxorubicin-loaded PLA-based MB, prepared by a different synthetic procedure (i.e. using a double emulsion polymerization technique), which also did not differ in size from drug-free MB [32]. Two-photon laser scanning microscopy (TPLSM) confirmed the entrapment of both model drugs in the polymeric shell of the MB (Fig. 3). Both the 1-step and the 2-step procedure led to significant amounts of Rhodamine-B and Coumarin-6 in the shell, confirming that the shell-thickness of PBCA-based MB is highly suitable for drug loading, and exemplifying that with shell thicknesses of 2–10% of the total MB diameter, polymer-based MB are much more suitable for drug delivery purposes than phospholipid-based MB, which have shell thicknesses of ~0.3% of their diameter. TPLSM furthermore confirmed an average size of ~1.5 μm and a relatively low polydispersity (Fig. 3).

3.2. Drug payload and encapsulation efficiency

A comparison between the number of Rhodamine-B and Coumarin-6 molecules encapsulated within the shell of PBCA MB upon 1-step and 2-step model drug loading is presented in Fig. 4. For Rhodamine-B, the 2-step procedure was more efficient at low feed ratios, while similar amounts were incorporated at higher feed ratios (i.e. at 1.5 and 5 mg). For Coumarin-6, the 2-step procedure was more efficient at all feed ratios. When compared to each other, independent of the mode of model drug loading, Coumarin-6 turned out to be much more suitable for incorporation into the shell of polymer-based MB than Rhodamine-B. This is in line with the observation of Wheatley and colleagues that highly hydrophobic drugs, such as paclitaxel, are entrapped much more efficiently into the shell of polymer-based MB than less hydrophobic drugs, such as doxorubicin [34]. Besides hydrophobicity, an additional aspect which likely plays an important role in this regard is the size/molecular weight (MW) of the model drugs. Since Coumarin-6 is ~30% smaller than Rhodamine-B, it seems likely that also due to this reduced size, significantly ($p<0.0001$) higher amounts of the former were incorporated, especially upon 2-step drug loading.

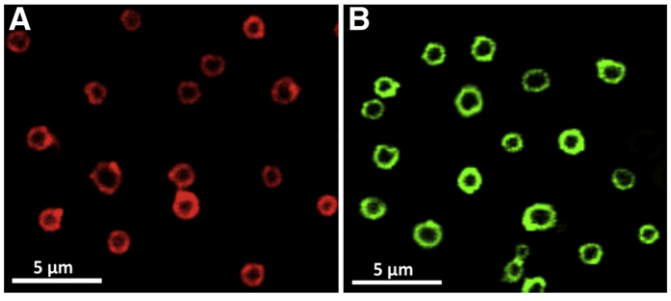

Fig. 3. Two-photon laser scanning microscopy images of PBCA-based MB loaded with Rhodamine-B (A) and Coumarin-6 (B), exemplifying efficient model drug incorporation into the MB shell, an average size of ~1.5 μm and a relatively low polydispersity.

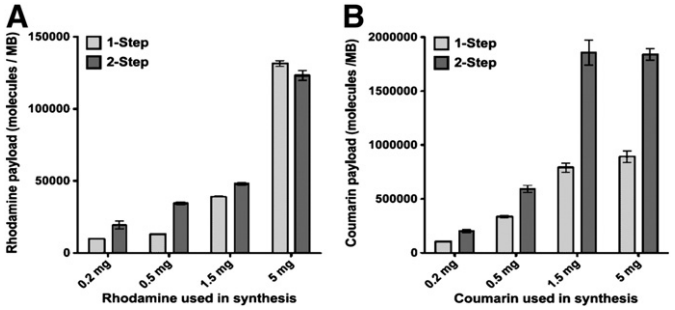

Fig. 4. Analysis of the number of model drug molecules incorporated into the shell of polymer-based MB upon 1-step and 2-step loading, exemplifying that hydrophobic fluorophores, such as Coumarin-6 (B) are entrapped much more efficiently than hydrophilic fluorophores, such as Rhodamine-B (A). Values represent average ± SD (n = 3).

The encapsulation efficiencies (EE) of Rhodamine-B and Coumarin-6 into the shell of PBCA-based MB are presented in Table 1, both in percent and in μg dye/mg shell material. Because of the definition of the EE (i.e. amount of model drug incorporated/amount of model drug added × 100%), values were always found to be significantly higher for the 2-step procedure as compared to the 1-step procedure ($p<0.05$). This is due to the fact that although equivalent amounts of fluorophore were used in both procedures, in the 1-step procedure, the model drugs were added to 300 mL of forming MB, while in the 2-step procedure, they were added to 20 mL of preformed MB. Consequently, in the 1-step procedure, the model drug molecules get entrapped in MB as well as in PBCA nanoparticles generated during the synthesis. However, these nanoparticles, together with non-encapsulated model drugs, are washed out during flotation. It therefore seems logical that in case of the 1-step procedure, substantially lower overall amounts of model drug are incorporated than in case of the 2-step procedure. When comparing the EE obtained for Rhodamine-B with those observed for Coumarin-6, significantly higher values were obtained for the latter, both upon 1-step and upon 2-step drug loading (see Fig. 2; $p<0.01$). This is in line with the notion that the polymeric shell of PBCA-based

Table 1
Encapsulation efficiency of Rhodamine-B and Coumarin-6 in PBCA-based MB.

	Amount added	Rhodamine-B		Coumarin-6	
		%	μg dye/mg shell	%	μg dye/mg shell
1-Step	0.2 mg	5.1 ± 0.11%	0.1 ± 0.01	38.3 ± 0.8%	0.5 ± 0.01
	0.5 mg	3.4 ± 0.03%	0.1 ± 0.01	35.0 ± 1.8%	1.6 ± 0.06
	1.5 mg	1.8 ± 0.03%	0.3 ± 0.01	26.8 ± 2.0%	3.8 ± 0.20
	5 mg	2.8 ± 0.04%	0.9 ± 0.02	17.9 ± 0.8%	4.3 ± 0.25
2-Step	0.2 mg	14.1 ± 2.3%	0.1 ± 0.02	45.6 ± 1.3%	1.0 ± 0.07
	0.5 mg	10.1 ± 0.4%	0.2 ± 0.01	53.0 ± 0.6%	2.9 ± 0.17
	1.5 mg	4.7 ± 0.1%	0.3 ± 0.01	55.6 ± 0.2%	9.0 ± 0.55
	5 mg	3.6 ± 0.1%	0.8 ± 0.02	16.5 ± 0.1%	8.9 ± 0.26

MB is hydrophobic, as well as with the study by Cochran et al. showing that paclitaxel is more efficiently incorporated into the shell of PLA-based MB than is doxorubicin [34].

With regard to the actual MB payload (μg dye/mg shell material), while similar amounts were determined for 1- and 2-step loading of Rhodamine-B, the amount of encapsulated Coumarin-6 doubled for 2-step compared to 1-step loading. Furthermore, approximately 5 times more Coumarin-6 could be incorporated by the 1-step synthesis compared to Rhodamine-B, while a 10-fold difference was observed for the 2-step synthesis. Wheatley and colleagues reported similar results, where they observed a 10-fold increase in the encapsulation of hydrophobic drugs (paclitaxel) compared to more hydrophilic drugs (doxorubicin) [34]. The absolute values in these studies are approximately a 10-fold higher than those reported here, which can be attributed to differences in synthetic protocols, in the shell thickness of the MB used and in the hydrophobicity of the agents encapsulated.

3.3. Effect of surface hydrolysis on MB payload

For Rhodamine-B-containing MB, the amount of model drug molecules incorporated into the shell of PBCA MB before and after surface hydrolysis did not change (Fig. 5A). For Coumarin-6, on the other hand, the number of model drug molecules per MB decreased upon surface hydrolysis (Fig. 5B; $p<0.001$). This is likely due to the fact that the introduction of carboxyl groups in the shell of PBCA MB leads to a substantial decrease in its hydrophobicity, and thereby to the loss of a substantial amount (~50%) of Coumarin-6 molecules from the MB shell. Comparing the acoustic properties of regular MB to those of model drug-loaded MB and hydrolyzed model drug-loaded MB showed that all formulations were equally efficient in generating US signals (Fig. 5C–D). This demonstrates that fluorophore encapsulation does not affect shell thickness and elasticity, which are the most important parameters for assuring proper US signal enhancement and US-triggered MB destruction. This is one of the major advantages of the loading strategies presented here over strategies involving the thickening of the MB shell with an oil layer to enable efficient drug encapsulation [40].

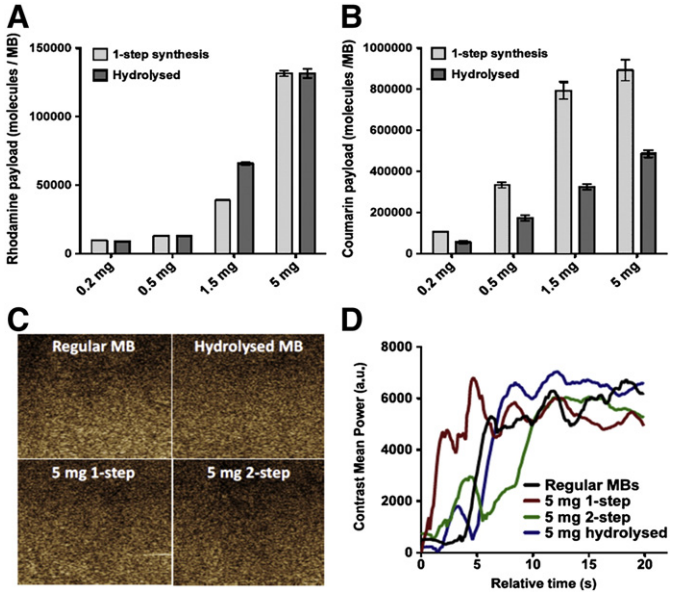

Fig. 5. Evaluation of the effect of MB surface-hydrolysis on the payload of Rhodamin-B (A) and Coumarin-6 (B). Values represent average ± SD (n = 3). Panels C and D exemplify that surface-hydrolysis and model drug-loading do not affect the US contrast enhancement properties of the MB.

Table 2
US-induced release of Rhodamine-B and Coumarin-6 from PBCA-based MB.

US-induced model drug release		
Amount added	Rhodamine-B	Coumarin-6
0.2 mg	75.2 ± 1.0%	77.8 ± 2.2%
0.5 mg	80.9 ± 6.9%	80.6 ± 6.4%
1.5 mg	80.8 ± 11.9%	82.6 ± 15.1%
5 mg	80.3 ± 1.7%	78.3 ± 7.9%

3.4. Quantification of US-triggered model drug release

When subsequently analyzing model drug release upon US treatment, it was found that 75–83% of the total amount of fluorophore molecules incorporated into the shell of PBCA-based MB was liberated (Table 2). No significant differences were observed between the relative amounts of model drug release for Rhodamine-B vs. Coumarin-6 loaded MB and for the 1-step vs. the 2-step loading procedures. Taking into account, however, that much higher absolute amounts of model drug were incorporated for Coumarin-6 as compared to Rhodamine-B (Fig. 4), and that consequently much higher overall numbers of model drugs were released for the former, it seems reasonable to conclude on the basis of these results, that hydrophobic agents are (much) more suitable for MB-mediated and US-triggered drug delivery than are hydrophilic agents.

3.5. Image-guided MB targeting to the tumor vasculature

Next, efficient US contrast enhancement and VEGFR2-mediated MB targeting to tumor blood vessels was validated in vivo. To this end, both model drug-loaded MB formulations were administered i.v. into CT26 tumor-bearing mice. Prior to i.v. injection, no non-linear contrast mode signals were detected within the tumor ROI (Fig. 6A). Immediately after MB injection, on the other hand, a strong signal enhancement was observed within the tumor region, confirming not only that the tumors used were properly perfused, but also that the acoustic properties of the model drug-loaded MB are

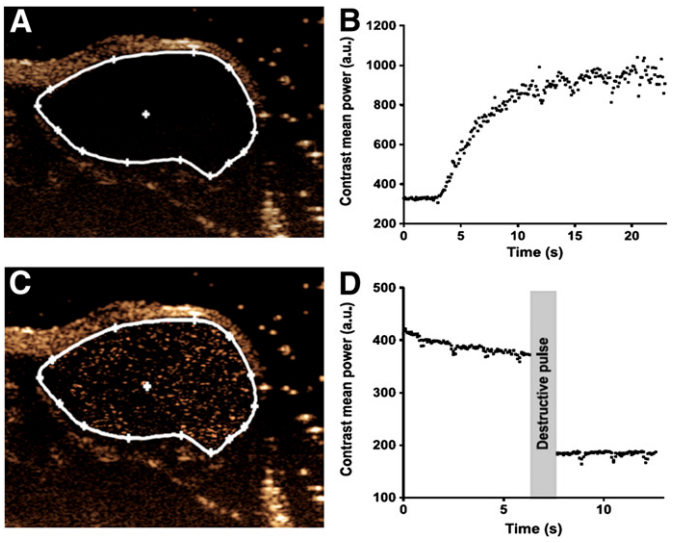

Fig. 6. Image-guided MB targeting to tumor endothelium. A subcutaneous CT26 tumor before MB administration is shown in panel A. After MB injection, the inflow of (Rhodamine-B-loaded) could be monitored non-invasively in non-linear contrast mode, confirming efficient tumor perfusion (B). Seven minutes after MB administration, a significant amount of VEGFR2-targeted MB was observed within the tumor (C). Comparing the contrast intensity in the tumor before (representing both circulating and bound MB) and after (only circulating MB) a high mechanical index destructive US pulse confirmed that the vast majority of MB present within the tumor 7 min p.i. were bound to tumor blood vessels (D).

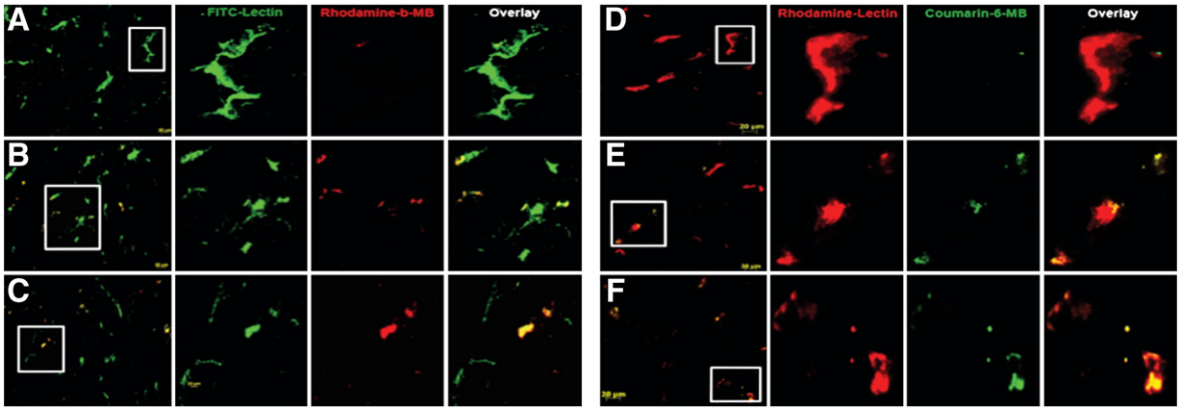

Fig. 7. Fluorescence microscopy analysis of Rhodamine-B (A–C) and Coumarin-6 (D–F) accumulation in tumors and tumor blood vessels upon US-mediated triggered model drug release from VEGFR2-targeted PBCA MB. In control animals, which were not exposed to US, hardly any Rhodamine-B and Coumarin-6 accumulation and extravasation could be observed (A, D). In animals treated with US 7 min after MB administration (B, E), as well as in animals continuously exposed to US (C, F), significant model drug release, accumulation and/or extravasation was observed. In A–C, Rhodamine-B is depicted in red, and FITC-lectin-stained blood vessels in green. In D–F, Coumarin-6 is depicted in green, and Rhodamine-lectin-stained blood vessels in red.

suitable for image-guided drug delivery (Fig. 6B). Seven min after injection, a significant number of MB were found to have bound to tumor endothelium (Fig. 6C). This time point was chosen as the circulation half-life time of PBCA is ~1 min (due to their rapid clearance by means of the reticuloendothelial system [41]), which implies that after 7 min, less than 1% of MB are still present in the blood. This notion is confirmed by the destruction-replenishment curve in Fig. 6D, which shows that after a high-mechanical index destructive US pulse, no inflow takes place, thereby validating that all MB present within the tumor ROI prior to the destructive pulse are bound to tumor blood vessels.

3.6. US-triggered model drug release from MB in vivo

In the final set of experiments, the tumor accumulation and in vivo release of Rhodamine-B and Coumarin-6 from VEGFR2-targeted PBCA MB upon exposure to high-mechanical index destructive US pulses were investigated. As shown in Fig. 7A and D, in animals not exposed to US, several intact MB were observed using fluorescence microscopy, but the overall amount of model drug accumulation and/or deposition was low. In animals exposed to three destructive US pulses 7 min after MB administration (Fig. 7B and E), on the other hand, as well as in animals continuously exposed to US (i.e. for 7 min; Fig. 7C and F), substantial amounts of accumulation and/or extravasation were observed.

It remains to be evaluated whether also in vivo, the signals observed in and around the tumor blood vessels upon US exposure result mostly from released model drugs (as in vitro), or mostly from fluorophores still present within extravasated and/or blood vessel-associated polymer fragments. Both scenarios might be interesting from a drug delivery point of view, with the former leading to a large burst release of drug molecules immediately after US triggering, and with the latter resulting in sustained drug release from extravasated and/or blood vessel-bound polymer fragments over time. Together with the promising results reported by Van Wamel, De Jong and colleagues on endothelial cell permeabilization [17,42–44], by McDannold, Hynynen and colleagues on BBB permeabilization [28,30], and by – among others – Ferrara, Wheatley, Frenkel, Klibanov, Sanders and colleagues on US-assisted and MB-mediated drug and gene delivery in general [18–23,26,27,32–34], these findings strongly urge for further (especially in vivo) efforts in this area of research.

4. Conclusion

Using two different synthetic strategies, PBCA-based polymeric MB were loaded with hydrophilic (Rhodamine-B) and hydrophobic (Coumarin-6) model drugs. Both model drugs could be entrapped relatively efficiently within the shell of the MB, but a clear preference was observed for incorporating hydrophobic agents. Hydrolyzing the surface of the MB and introducing anti-VEGFR2-antibodies did not affect Rhodamine-B-loading, but lowered the payload of Coumarin-6, by ~50%, likely due to increases in the hydrophilicity of the MB shell. Model drug incorporation did not negatively affect the acoustic properties of the MB. VEGFR2-targeted and fluorophore-loaded MB were shown to be highly suitable for image-guided drug targeting to tumor blood vessels, and to release significant amounts of both model drugs (~80%) upon exposure to high-mechanical index destructive US pulses. Consequently, antibody-modified and polymer-based MB seem to be highly suitable systems for image-guided, targeted and triggered drug delivery to tumors and tumor blood vessels.

Acknowledgments

The authors gratefully acknowledge financial support by the DFG (KI 1072/5-1; KI 1072/8-1; LA 2937/1-1), by the EC (COST-Action TD1004) and by Hightech.NRW (ForSaTum).

References

[1] H. Maeda, J. Wu, T. Sawa, Y. Matsumura, K. Hori, Tumor vascular permeability and the EPR effect in macromolecular therapeutics: a review, J. Controlled Release 65 (2000) 271–284.
[2] M.E. Davis, Z.G. Chen, D.M. Shin, Nanoparticle therapeutics: an emerging treatment modality for cancer, Nat. Rev. Drug Discov. 7 (2008) 771–782.
[3] D. Peer, J.M. Karp, S. Hong, O.C. Farokhzad, R. Margalit, R. Langer, Nanocarriers as an emerging platform for cancer therapy, Nat. Nanotechnol. 2 (2007) 751–760.
[4] T. Lammers, W.E. Hennink, G. Storm, Tumour-targeted nanomedicines: principles and practice, Br. J. Cancer 99 (2008) 392–397.
[5] R.K. Jain, T. Stylianopoulos, Delivering nanomedicine to solid tumors, Nat. Rev. Clin. Oncol. 7 (2010) 653–664.
[6] R. Duncan, R. Gaspar, Nanomedicine(s) under the microscope, Mol. Pharm. 8 (2011) 2101–2141.
[7] T. Lammers, F. Kiessling, W.E. Hennink, G. Storm, Drug targeting to tumors: Principles, pitfalls and (pre-) clinical progress, J. Controlled Release 161 (2012) 175–187.
[8] N. Kumar, R.S. Langer, A.J. Domb, Polyanhydrides: an overview, Adv. Drug Delivery Rev. 54 (2002) 889–910.
[9] M.A. Moses, H. Brem, R. Langer, Advancing the field of drug delivery: taking aim at cancer, Cancer Cell 4 (2003) 337–341.
[10] H. Okada, H. Toguchi, Biodegradable microspheres in drug delivery, Crit. Rev. Ther. Drug Carrier Syst. 12 (1995) 1–99.
[11] A.L. Lewis, M.R. Dreher, Locoregional drug delivery using image-guided intra-arterial drug eluting bead therapy, J. Controlled Release 161 (2012) 328–350.
[12] J.R. Lindner, Microbubbles in medical imaging: current applications and future directions, Nat. Rev. Drug Discov. 3 (2004) 527–532.

[13] A.L. Klibanov, Ligand-carrying gas-filled microbubbles: ultrasound contrast agents for targeted molecular imaging, Bioconjug. Chem. 16 (2005) 9–17.
[14] F. Kiessling, J. Huppert, M. Palmowski, Functional and molecular ultrasound imaging: concepts and contrast agents, Curr. Med. Chem. 16 (2009) 627–642.
[15] E.C. Unger, E. Hersh, M. Vannan, T.O. Matsunaga, T. McCreery, Local drug and gene delivery through microbubbles, Prog. Cardiovasc. Dis. 44 (2001) 45–54.
[16] S. Mitragotri, Healing sound: the use of ultrasound in drug delivery and other therapeutic applications, Nat. Rev. Drug Discov. 4 (2005) 255–260.
[17] A. van Wamel, K. Kooiman, M. Harteveld, M. Emmer, F.J. ten Cate, M. Versluis, N. de Jong, Vibrating microbubbles poking individual cells: drug transfer into cells via sonoporation, J. Controlled Release 112 (2006) 149–155.
[18] K. Ferrara, R. Pollard, M. Borden, Ultrasound microbubble contrast agents: fundamentals and application to gene and drug delivery, Annu. Rev. Biomed. Eng. 9 (2007) 415–447.
[19] V. Frenkel, Ultrasound mediated delivery of drugs and genes to solid tumors, Adv. Drug Delivery Rev. 60 (2008) 1193–1208.
[20] S. Hernot, A.L. Klibanov, Microbubbles in ultrasound-triggered drug and gene delivery, Adv. Drug Delivery Rev. 60 (2008) 1153–1166.
[21] K.W. Ferrara, M.A. Borden, H. Zhang, Lipid-shelled vehicles: engineering for ultrasound molecular imaging and drug delivery, Acc. Chem. Res. 42 (2009) 881–892.
[22] I. Lentacker, S.C. De Smedt, N.N. Sanders, Drug loaded microbubble design for ultrasound triggered delivery, Soft Matter 5 (2009).
[23] A.L. Klibanov, T.I. Shevchenko, B.I. Raju, R. Seip, C.T. Chin, Ultrasound-triggered release of materials entrapped in microbubble-liposome constructs: a tool for targeted drug delivery, J. Controlled Release 148 (2010) 13–17.
[24] R. Deckers, A. Yudina, L.C. Cardoit, C.T. Moonen, A fluorescent chromophore TOTO-3 as a 'smart probe' for the assessment of ultrasound-mediated local drug delivery in vivo, Contrast Media Mol. Imaging 6 (2011) 267–274.
[25] L.H. Treat, N. McDannold, N. Vykhodtseva, Y. Zhang, K. Tam, K. Hynynen, Targeted delivery of doxorubicin to the rat brain at therapeutic levels using MRI-guided focused ultrasound, Int. J. Cancer 121 (2007) 901–907.
[26] I. Lentacker, B. Geers, J. Demeester, S.C. De Smedt, N.N. Sanders, Design and evaluation of doxorubicin-containing microbubbles for ultrasound-triggered doxorubicin delivery: cytotoxicity and mechanisms involved, Mol. Ther. 18 (2010) 101–108.
[27] R.E. Vandenbroucke, I. Lentacker, J. Demeester, S.C. De Smedt, N.N. Sanders, Ultrasound assisted siRNA delivery using PEG-siPlex loaded microbubbles, J. Controlled Release 126 (2008) 265–273.
[28] M. Kinoshita, N. McDannold, F.A. Jolesz, K. Hynynen, Noninvasive localized delivery of Herceptin to the mouse brain by MRI-guided focused ultrasound-induced blood–brain barrier disruption, Proc. Nat. Acad. Sci. U. S. A. 103 (2006) 11719–11723.
[29] M. Stroick, A. Alonso, M. Fatar, M. Griebe, S. Kreisel, R. Kern, E. Gaud, M. Arditi, M. Hennerici, S. Meairs, Effects of simultaneous application of ultrasound and microbubbles on intracerebral hemorrhage in an animal model, Ultrasound Med. Biol. 32 (2006) 1377–1382.
[30] K. Hynynen, Ultrasound for drug and gene delivery to the brain, Adv. Drug Delivery Rev. 60 (2008) 1209–1217.
[31] F. Kiessling, S. Fokong, P. Koczera, W. Lederle, T. Lammers, Ultrasound Microbubbles for Molecular Diagnosis, Therapy and Theranostics, J. Nucl. Med. 53 (2012) 345–348.
[32] J.R. Eisenbrey, O.M. Burstein, R. Kambhampati, F. Forsberg, J.-B. Liu, M.A. Wheatley, Development and optimization of a doxorubicin loaded poly(lactic acid) contrast agent for ultrasound directed drug delivery, J. Controlled Release 143 (2010) 38–44.
[33] J.R. Eisenbrey, M.C. Soulen, M.A. Wheatley, Delivery of encapsulated Doxorubicin by ultrasound-mediated size reduction of drug-loaded polymer contrast agents, IEEE Trans. Biomed. Eng. 57 (2010) 24–28.
[34] M.C. Cochran, J. Eisenbrey, R.O. Ouma, M. Soulen, M.A. Wheatley, Doxorubicin and paclitaxel loaded microbubbles for ultrasound triggered drug delivery, Int. J. Pharm. 414 (2011) 161–170.
[35] M. Palmowski, J. Huppert, P. Hauff, M. Reinhardt, K. Schreiner, M.A. Socher, P. Hallscheidt, G.W. Kauffmann, W. Semmler, F. Kiessling, Vessel fractions in tumor xenografts depicted by flow- or contrast-sensitive three-dimensional high-frequency Doppler ultrasound respond differently to antiangiogenic treatment, Cancer Res. 68 (2008) 7042–7049.
[36] M. Palmowski, J. Huppert, G. Ladewig, P. Hauff, M. Reinhardt, M.M. Mueller, E.C. Woenne, J.W. Jenne, M. Maurer, G.W. Kauffmann, W. Semmler, F. Kiessling, Molecular profiling of angiogenesis with targeted ultrasound imaging: early assessment of antiangiogenic therapy effects, Mol. Cancer Ther. 7 (2008) 101–109.
[37] M. Palmowski, P. Peschke, J. Huppert, P. Hauff, M. Reinhardt, M. Maurer, C.P. Karger, M. Scholz, W. Semmler, P.E. Huber, F.M. Kiessling, Molecular ultrasound imaging of early vascular response in prostate tumors irradiated with carbon ions, Neoplasia 11 (2009) 856–863.
[38] S. Fokong, M. Siepmann, Z. Liu, G. Schmitz, F. Kiessling, J. Gatjens, Advanced characterization and refinement of poly N-butyl cyanoacrylate microbubbles for ultrasound imaging, Ultrasound Med. Biol. 37 (2011) 1622–1634.
[39] M. Palmowski, B. Morgenstern, P. Hauff, M. Reinhardt, J. Huppert, M. Maurer, E.C. Woenne, S. Doerk, G. Ladewig, J.W. Jenne, S. Delorme, L. Grenacher, P. Hallscheidt, G.W. Kauffmann, W. Semmler, F. Kiessling, Pharmacodynamics of streptavidin-coated cyanoacrylate microbubbles designed for molecular ultrasound imaging, Invest. Radiol. 43 (2008) 162–169.
[40] K. Kooiman, M.R. Bohmer, M. Emmer, H.J. Vos, C. Chlon, W.T. Shi, C.S. Hall, S.H. de Winter, K. Schroen, M. Versluis, N. de Jong, A. van Wamel, Oil-filled polymer microcapsules for ultrasound-mediated delivery of lipophilic drugs, J. Controlled Release 133 (2009) 109–118.
[41] F. Forsberg, B.B. Goldberg, J.B. Liu, D.A. Merton, N.M. Rawool, W.T. Shi, Tissue-specific US contrast agent for evaluation of hepatic and splenic parenchyma, Radiology 210 (1999) 125–132.
[42] A. van Wamel, A. Bouakaz, M. Versluis, N. de Jong, Micromanipulation of endothelial cells: ultrasound-microbubble-cell interaction, Ultrasound Med. Biol. 30 (2004) 1255–1258.
[43] A. van Wamel, K. Kooiman, M. Emmer, F.J. ten Cate, M. Versluis, N. de Jong, Ultrasound microbubble induced endothelial cell permeability, J. Controlled Release 116 (2006) e100–e102.
[44] K. Kooiman, M. Emmer, M. Foppen-Harteveld, A. van Wamel, N. de Jong, Increasing the endothelial layer permeability through ultrasound-activated microbubbles, IEEE Trans. Biomed. Eng. 57 (2010) 29–32.